

Energy balance in a large compartment fire

Anthony Hamins*, Erik Johnsson, Michelle Donnelly, Alexander Maranghides

Building and Fire Research Laboratory, National Institute of Standards and Technology, 100 Bureau Drive, Stop 8663, Gaithersburg, MD 20899-8663, USA

Received 27 September 2006; received in revised form 3 July 2007; accepted 8 August 2007

Available online 21 September 2007

Abstract

The National Institute of Standards and Technology (NIST) and the Nuclear Regulatory Commission (NRC) are collaborating to assess and validate fire computer codes for nuclear power plant applications. This evaluation is being conducted through a series of benchmarking and validation exercises. The goal of the present study was to provide data from a large-scale fire test of a simulated nuclear power plant cable room. The experiments consisted of a hydrocarbon spray fire with a 1 MW heat release rate, burning in a single compartment 7 m wide, 22 m long, and 4 m high. Measurements included the vertical temperature profiles, heat flux to the compartment surfaces, the velocity and temperature at the compartment doorway, and the total heat release rate. From these measurements, an energy balance was considered, in which it was determined that nearly 74% of the fire's energy went to heat compartment surfaces, 22% escaped through the doorway, and 4% heated gases in the compartment.

Published by Elsevier Ltd.

Keywords: Compartment fire; Energy balance; Fire experiments; Model validation

1. Introduction

Consideration of the conservation of energy is a key tenet of engineering. In this study, this principle is considered for a fire in a compartment, with emphasis on tracking changes in the thermal environment. Quantitatively understanding the distribution of energy released by a fire is important for testing the accuracy of computational fire codes, which are used to design fire protection systems through simulation of the thermal environment associated with a fire.

Conservation of energy holds that the transient fire heat release rate ($\dot{Q}_f(t)$) goes to heat the gases within the compartment ($\dot{Q}_g(t)$), is transferred to compartment surfaces by radiation and convection ($\dot{Q}_w(t)$), and is transported through the doorway ($\dot{Q}_d(t)$):

$$\dot{Q}_f(t) = \dot{Q}_g(t) + \dot{Q}_w(t) + \dot{Q}_d(t). \quad (1)$$

Textbooks and fire models consider the distribution and conservation of energy in compartment fires. The models are based on experiments that have explicitly tracked the

partition of energy associated with a fire [1]. The experimental study presented here considers the energy balance in a large compartment with an emphasis on measurement uncertainty, which is essential for model validation. The objective of this study was to gain confidence in the accuracy of each of the component measurements that are considered in an energy balance. Conservation of energy is a check on the accuracy of the individual measurements and lends confidence to quality of the data.

This paper focuses on two of a series of experiments (Test 3 and a replicate experiment, Test 9, in Ref. [2]) that were conducted to provide data to evaluate the accuracy of zone models, computational fluid dynamic fire models, and simple fire correlations [3,4]. The test series was designed to provide a comprehensive data set in which the experiment and the boundary conditions were fully defined and characterized for subsequent comparison with models. The experiments described here were selected as illustrative of the measurement approach used to track the time-varying enthalpy and its distribution, for a fire in a large geometrically simple compartment.

Measurements in this study focused on the fire behavior and the thermal environment. The nominal heat release

*Corresponding author. Tel.: +1 301 975 6598; fax: +1 301 975 4052.
E-mail address: anthony.hamins@nist.gov (A. Hamins).

Nomenclature			
A_i	area of the i th section in the doorway	$\dot{Q}_w(t)$	enthalpy transferred to compartment surfaces
C_p	temperature dependent gas heat capacity	TC	thermocouple
H_c	heat of combustion of the fuel	T_i	temperature at location i
K	factor in the bidirectional probe calibration	v_i	gas velocity at location i
\dot{m}	mass burning rate		
M	molecular weight		<i>Greek symbols</i>
P_{absolute}	absolute barometric pressure	Δp	differential pressure
\dot{q}_i''	heat flux to compartment surface or heat flux gauge	ΔT_i	increase in temperature above ambient at location i
R	universal gas constant	ε	emissivity of the compartment surface or heat flux gauge
$\dot{Q}_f(t)$	actual heat release rate of the fire	ρ	gas density
$\dot{Q}_g(t)$	enthalpy to heat gases within the compartment	ρ_i	gas density at location i
$\dot{Q}_d(t)$	enthalpy transported through the doorway	σ	Stefan–Boltzmann constant

rate of the fire was 1 MW, with the burner located at the center of a large compartment. The heat release rate was measured using calorimetry. A single door to the compartment was open during the experiment, and the flow field was characterized using an array of bidirectional probes. The heat loss to the compartment surfaces was measured using an array of sensors placed at select locations on the compartment walls, floor, and ceiling.

Several measurements were made before the experiments began, including compartment leakage, and the thermal and optical properties of the surface materials. In addition, the combustion properties and behavior of the test fuel were characterized in a separate series of experiments that measured the heat of combustion, the combustion efficiency, the radiative fraction, and the yields of soot, CO₂, and CO for the same burner as used in the experiments described here [5].

More than 350 instruments were used to make measurements during the experimental series. This paper focuses on those measurements that were important to understand the enthalpy balance and the thermal environment in the compartment, including measurements of:

- Vertical profiles of temperature.
- The heat release rate through oxygen consumption calorimetry.
- Total heat loss to the compartment walls, ceiling, and floor.
- Total mass and heat flux through the compartment door.

Other measurements are described in Ref. [3] and included the soot density, the concentrations of oxygen, carbon monoxide, and carbon dioxide in the hot gas layer, the compartment pressure, the radiative and total heat flux at various targets in the compartment, surface and core temperatures of horizontally and vertically oriented control and power cables, and visible and infrared video records from multiple perspectives. Measurements were made

before the test began and after the fuel was stopped to assure documentation of the measurement baseline as a reference. Data were acquired at a sampling rate of 1 Hz. The remainder of this paper describes the experimental configuration and conditions, the experimental apparatus and procedures, and the measurement results.

2. Experimental configuration and conditions

2.1. Test compartment

Fig. 1 shows the test compartment, which was 7.04 m × 21.66 m × 3.82 m ($W \times L \times H$) in size, designed to represent a realistic-scale cable room in a nuclear power plant. The total compartment volume was 582 m³. A 2.0 m by 2.0 m doorway was located on the middle of the west wall (7.04 m) of the compartment. The compartment walls and ceiling were covered with two layers of calcium silicate boards (“marinite”¹) each layer 0.0125 m ($\frac{1}{2}$ in) thick, while the floor was covered with one layer of 0.0125 m ($\frac{1}{2}$ in) thick gypsum board on top of a 0.0183 m (0.72 in) layer of plywood. Thermophysical and optical properties of the marinate and other materials used in the compartment are given in Ref. [2].

The ambient humidity and temperature during the test were measured as 34% ± 10% and 30 °C ± 2 °C, respectively. The uncertainty in these quantities, as all uncertainties mentioned in this report, are expressed as the combined expanded uncertainty with an expansion factor equal to two (i.e., 2σ), which represents a 95% confidence interval. The combined uncertainty represents estimates of both measurement variance and measurement bias.

¹Certain commercial entities, equipment, or materials may be identified in this document in order to describe an experimental procedure or concept adequately. Such identification is not intended to imply recommendation or endorsement by the National Institute of Standards and Technology, nor is it intended to imply that the entities, materials, or equipment are necessarily the best available for the purpose.

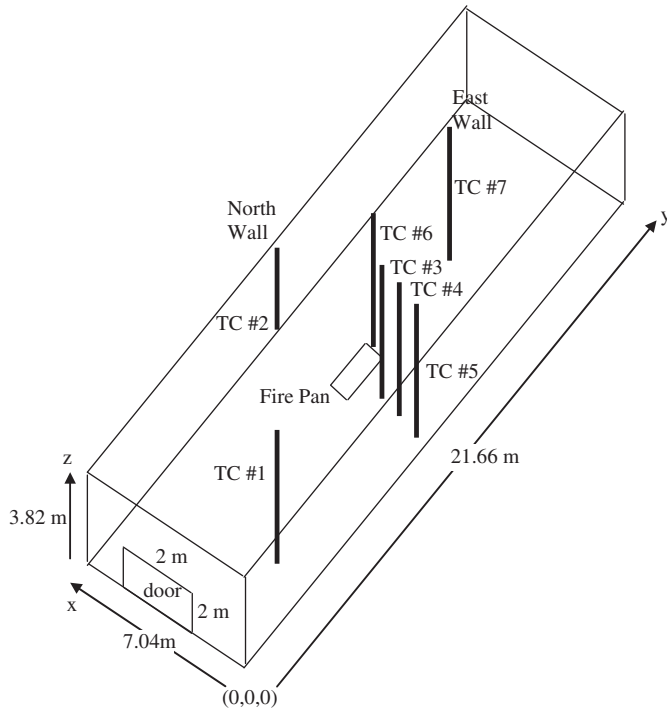


Fig. 1. Compartment layout with seven thermocouple trees.

2.2. Fuel delivery system and fire

The fuel used was a commercial mixture of heptane isomers. The fuel system consisted of a fuel storage container and a magnet driven positive displacement gear pump. The pump was controlled by an alternating current (AC) variable frequency driver. Fuel was delivered through a single 90° spray angle full-cone spray nozzle oriented downwards onto a 1.0 m by 2.0 m stainless steel pan with a 5 cm lip. The fire pan was located on the floor at the center of the compartment as shown in Fig. 1. The idealized heat release rate associated with the heptane fuel flow ($\dot{m} H_c$) was estimated as 1140 kW [2].

The fuel flow was composed of a 3 min ramp-up in a linear manner from zero to a long steady burning period, of 20 min duration, followed by a 3 min linear ramp-down to zero flow. The total fire duration was 26 min or 1560 s. Measurements of the fuel density and the heat of combustion per mass of oxygen consumed (used to interpret the calorimetry measurements) are described in Hamins et al. [5]. The values were almost the same as those of *n*-heptane.

3. Experimental apparatus and procedures

3.1. Gas temperatures and layer height

Gas temperatures were measured using seven thermocouple (TC) trees with each tree instrumented with 10 type-K (chromel-alumel) 24 gauge TCs spaced 35 cm apart, starting 35 cm from the floor and ending 32 cm from the ceiling. The TC beads were located on individual hor-

Table 1
Location of thermocouple Trees (refer to Fig. 1)

Tree number	Location (x,y)
1	5.00 m, 3.58 m
2	10.85 m, 6.85 m
3	10.85 m, 2.20 m
4	10.85 m, 1.35 m
5	10.85 m, 0.55 m
6	11.95 m, 3.58 m
7	16.70 m, 3.58 m

izontal “branches.” The trees were suspended from the ceiling and attached to the floor with a screw to provide tension to maintain vertical alignment. The exact TC locations are given in Table 1, where the reference location $(x,y) = (0,0)$, was the bottom right hand corner of the compartment as seen in Fig. 1.

The average temperature of the gas layers and the layer depth was calculated using the integral ratio method described in Ref. [7]. The vertical TC trees were used to determine the hot gas layer depth and temperature, except Tree 4, which had a faulty TC. The TC data were weighted because the TC trees were not evenly distributed within the compartment. The weighting factors considered the relative location of the TCs and were assigned based on representative floor area subtended by each tree. In addition, one of the thermocouples on Tree 4 malfunctioned during the test, so data from Tree 4 was discounted for determination of average layer temperature and depth. The relative weightings used in this study were 0.3, 0.2, 0.1, 0, 0.05, 0.05, and 0.3 for Trees 1–7, respectively. Calculations of the upper layer depth and temperature showed that a simple average of the TC tree measurements yielded results nearly identical to the weighted results (within 2%). The weighted average temperature was used to estimate the gas layer temperatures and layer height.

Aspirated TCs with a double shield stainless steel design (0.95 cm outer diameter), which suffer minimal radiative exchange [6] were used to calibrate the bare bead TC measurements at a limited number of locations. To generate sufficient velocity (approximately 10 m/s) and convective heat transfer over the bead of the aspirated TCs, flow through the probes was set to a minimum of 24 L/min.

3.2. Heat loss to surfaces

To estimate the total heat loss to the ceiling, floor, and walls of the test compartment, measurements of heat flux to the interior surfaces were conducted at numerous locations. The number of heat flux measurement locations was limited by resource availability. The selection of sensor type and its placement was optimized through analysis using computational fire modeling.

To determine how many measurements were necessary, an evaluation of sensor density versus uncertainty level was conducted. The National Institute of Standards and

Technology (NIST) Fire Dynamics Simulator (FDS) was used to model the enclosure with a 1 MW fire located in the center of the enclosure with the doorway open [8]. The model predicted the temperature and radiation fields at the interior surfaces of the enclosure. The effect of limiting the number and placement of sensors used in the calculation was analyzed relative to a baseline calculation that utilized a high density of sensors (hundreds of sensors). The calculation results were sensitive to the distribution pattern as well as the number of sensors. A non-uniform approach worked best with more sensors used in regions of high flux gradient and fewer sensors used where fluxes were more uniform [2].

Fig. 2 shows an uncooled heat flux gauge and its corresponding wall-mounted TC on the south wall. The net flux accounted for the incident total heat flux less re-radiation to the environment from the gauge (which is a function of the temperature and emissivity of the gauge). The net radiation to the compartment wall (not the sensor) was equal to the net flux to the gauge adjusted by the difference between the net flux to the gauge and to the adjacent wall material. This depended on the difference between the temperature and emissivity of the compartment surface and the gauge. For the two types of gauges, manufacturer-provided total emissivities (averaged over the infrared spectrum) were used. To estimate re-radiation from the compartment surfaces, the temperatures of the gauge, as well as the compartment surface near the gauge, were measured with type K TCs. The gauge temperature was generally lower than the adjacent surface temperature by a few degrees to tens of degrees. There were a few possible explanations for this. The gauge had a finite mass with the TC actually embedded within the gauge. This caused an additional heat capacity and time lag not experienced by the bare compartment surface. Although the heat flux gauges were attached with a conductive paste, the contact and level of conduction may not have allowed perfect thermal contact between the gauge and the surface. The quality of the surface TC installation, and its contact with the surface, may have also influenced the surface temperature measurement. Finally, near the fire and especially in the lower layer, the surface temperatures could have been overestimated by some amount due to radiative heating of the TC bead. Aspirated thermocouple

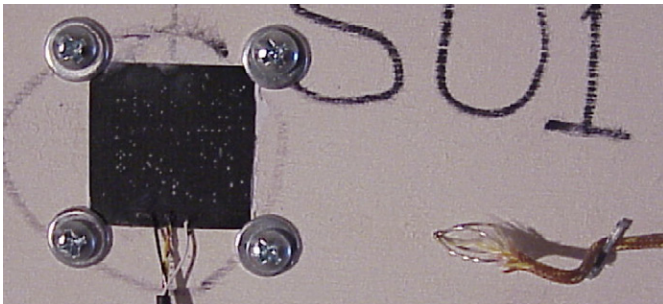


Fig. 2. A heat flux gauge and wall-mounted thermocouple on the south wall.

measurements provided estimates of that effect, suggesting that the lower layer TCs were accurate to within 30 °C.

For the calculation of heat loss to the enclosure, the wall gauge heat flux data were replaced with surface heat fluxes corrected for the temperature difference between the surfaces (T_{wall}) and gauges (T_{gauge}) according to the following equation:

$$\dot{q}''_{\text{wall}} = \dot{q}''_{\text{gauge}} - \varepsilon\sigma(T_{\text{wall}}^4 - T_{\text{gauge}}^4), \quad (2)$$

where \dot{q}''_{wall} is the heat flux to the compartment surface, \dot{q}''_{gauge} is the heat flux to the gauge, σ is the Stefan–Boltzmann constant, and ε is the emissivity of the compartment surface and the gauge, which were measured to be approximately equal [2]. The difference in the convective heat flux to the compartment surfaces and the gauge was assumed to be small. The heat flux to each of the surfaces was summed to determine the total energy loss rate to each of the surfaces (\dot{Q}_w).

3.2.1. Instrumentation

Preliminary FDS modeling of the experiment predicted heat fluxes to average about 2 kW/m² on the compartment walls with some regions reaching several times that value and much of the enclosure receiving less than 1 kW/m². Modeling also predicted surface temperatures greater than 150 °C on a relatively small portion of the ceiling near the fire, while the remaining surface temperatures were predicted to be less than 150 °C. Because of the temperature variations, different types of sensors were selected for the high and low temperature regions. Low cost, uncooled heat flux sensors were used in regions expected to remain below 150 °C. More expensive, high-temperature heat flux gauges were used in the higher flux regions near the fire.

The lower temperature gauge was a Vatel model BF-04 (rated to 150 °C) with an embedded K-type TC. The higher temperature gauge was an ITI Model C Polyamide Heat Flux Transducer (rated to 300 °C) with an embedded type-K TC. The gauges were mounted using Omega Engineering's Omegatherm thermally conductive high-temperature grease (model number OT-201). Fig. 2 the four 6-32 screws and washers that were used to press the corners of the heat flux gauge against the grease and prevent motion of the gauge due to heat-cycling. Each heat flux gauge had an associated, embedded TC to determine the surface temperature of the gauge and also one located approximately 5 cm away on the enclosure surface for comparison. The sensors were positioned in matching patterns with six gauges on both the north and the south walls, four gauges on both the east and the west walls, and eight gauges on both the ceiling and the floor. The total number of sensors used was 36 of which 8 were of the type rated for higher temperature. The exact sensor locations are listed in Ref. [2] for each of the compartment surfaces. To determine the heat loss through a surface, the surface was partitioned into representative areas or zones about each measurement station and the losses through each zone were summed.

3.2.2. Measurement uncertainty

The number of sensors used and their location pattern contributed to the uncertainty estimate for the flux to the compartment surfaces. Uncertainties associated with emissivities and the temperature measurements were also considered.

The heat flux gauges were factory calibrated with uncertainties of $\pm 3\%$. The factory calibration of each model type was verified at NIST. To check the calibration, an example of each type of gauge was mounted on a 30 cm square piece of the enclosure wall material and placed at a predetermined position in front of a radiant panel. The heat fluxes were compared to measurements made with a calibrated reference gauge. Since the gauge signal output changed during heating, the gauge temperature as well as the signal were measured. Contributors to the measurement uncertainty included the calibration, the temperature measurement, the emissivity, and the limited number of sensors. The total relative expanded uncertainty was estimated as 11% [2].

3.3. Doorway flows

To determine the mass and enthalpy flows into and out of the compartment doorway, measurements of the temperature and the gas velocity fields were conducted. Fourteen bidirectional probes [9] were placed in three vertical arrays in the doorway opening to determine the velocity profiles in the doorway. The instrument locations were essentially symmetric, in three columns, 20 cm from the sides of the door and along the centerline. The gauges were positioned 20 cm from the top and bottom of the door and then every 40 cm ($Z = 20, 60, 100, 140, 180$ cm). Bidirectional probes are relatively insensitive (to within $\pm 10\%$) to flow angle for angles within approximately $\pm 50^\circ$ of the probe axis [9] and were therefore suitable for doorway flows [10].

Gas temperature in the doorway was measured using type-K bare bead TCs positioned 1 cm above the center of each of the bidirectional probes. To confirm the bare-bead TC measurements, three aspirated TCs were placed in the doorway. The results of the aspirated TC measurements confirmed that the radiative flux from the fire (which was about 10 m away) and the hot upper layer did not impact the bare bead TC readings at the doorway.

The bidirectional probes were connected to differential pressure transducers, each with a maximum differential pressure measurement capability of 133 Pa. The transducers were calibrated using a water manometer oriented at a small angle off horizontal. The differential pressure, Δp , measured by each probe, and the temperature, T , at the corresponding probe location were used to compute the gas velocity, v , by the equation:

$$v = \frac{1}{K} \sqrt{\frac{2\Delta p}{\rho}}, \quad \text{where} \quad \rho = \frac{(M)P_{\text{absolute}}}{RT}. \quad (3)$$

In this computation, the density (ρ) was computed as a function of temperature using the ideal gas law. The gas was assumed to be pure air with a molecular weight (M) of 0.029 kg/mol. Here, P_{absolute} is the absolute barometric pressure and R is the universal gas constant. The K factor was taken as 1.08 as reported in Ref. [9]. The combined expanded uncertainty of the velocity measurements was estimated as ± 0.3 m/s, which was due mainly to scatter in the data and uncertainty in the calibration.

3.4. Oxygen consumption calorimetry

The fire heat release rate (\dot{Q}_f) was measured using oxygen consumption calorimetry in a 9 m by 12 m exhaust hood. The hot gases and smoke flowed from the compartment doorway and were captured by the exhaust hood. Bryant et al. [11] describe the NIST calorimetry instrumentation, calibration, measurement uncertainty and experimental procedures in detail. The calorimetry determination required about 40 measurements, including the volume fractions of O_2 , CO , CO_2 , and the average temperature and velocity in the exhaust duct. A correction was made for ambient humidity [11]. A natural gas burner with active flow control was employed in calibration burns to assure accurate determination of \dot{Q}_f . The heat output of the burner was held constant for 3–5 min at each setting. The measured \dot{Q}_f was typically within 11% of that expected based on the mass flow rate of the natural gas. The reasons for this difference were not certain, but may have been due, at least in part, to the nature of the flow field in the exhaust duct, where the velocity profile does not correspond to fully developed pipe flow at the downstream measurement station. The calorimetry results were corrected based on this calibration factor [2]. The combined expanded relative measurement uncertainty was estimated as 15% [2]. The calorimetry measurement response time was on the order of 15 s [11]. The volume of the test compartment also affected the time response of this measurement, as filling and mixing caused averaging and lag in the calorimetry results.

4. Discussion of results

4.1. Gas temperature and layer height

Fig. 3 shows bare bead TC measurements as a function of time on Tree 7, which was located 6 m from the fire toward the center of the east wall. The temperature profiles differed depending on position. Fig. 4 shows the top TC on the various trees as well as the calculated weighted average (see Table 1 and Fig. 1 for TC locations). Tree 6, which was very close to the fire, had relatively high temperatures.

Estimates of the mean temperature of the upper and lower gas layers, and the layer height were based on the average temperature data using the integral ratio method [7]. The measured temperature and the layer height as a function of time are shown in Fig. 5. The temperature of

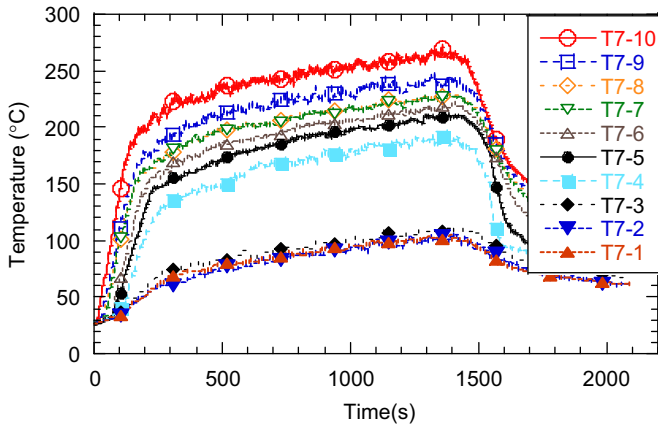


Fig. 3. Thermocouple temperature measurements as a function of time on Tree 7.

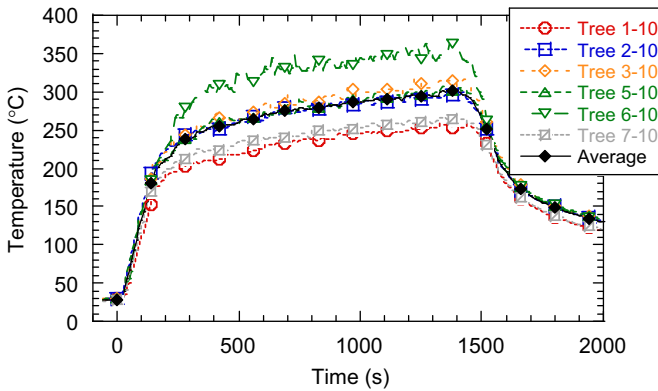


Fig. 4. Thermocouple temperature measurements as a function of time for the top thermocouple on Trees 1–7 and their weighted average value.

both the upper and the lower layer increased with time, with the upper and lower layers reaching temperatures as large as 270 °C and 100 °C, respectively. The location of the upper layer rapidly moved from the ceiling to 1.2 m above the floor, somewhat below the top of the doorway.

The power that went to heat the gases in the compartment volume, denoted here as \dot{Q}_g , was related to the time derivative of the change in enthalpy of the gases. This was approximated as the sum of the enthalpy change in the upper and lower gas layers:

$$\dot{Q}_g(t) \cong \frac{d}{dt} \sum_{i=1}^2 (\rho_i \cdot V_i \cdot C_p \cdot \Delta T_i), \quad (4)$$

where ρ_i is the time dependent gas density of the upper or lower layer ($i = 1$ or 2) of volume V_i , C_p is the temperature dependent gas heat capacity (taken to be that of air), and ΔT_i is the increase in temperature from ambient. The value of \dot{Q}_g was calculated using the data shown in Fig. 5 and Eq. (4).

The estimated uncertainty of \dot{Q}_g in Eq. (4) considered uncertainty in the temperature measurements. Aspirated TC measurements made in the upper and lower layer (near TCs 3 and 8 on Tree 5; at 1.05 m and 2.80 m, respectively,

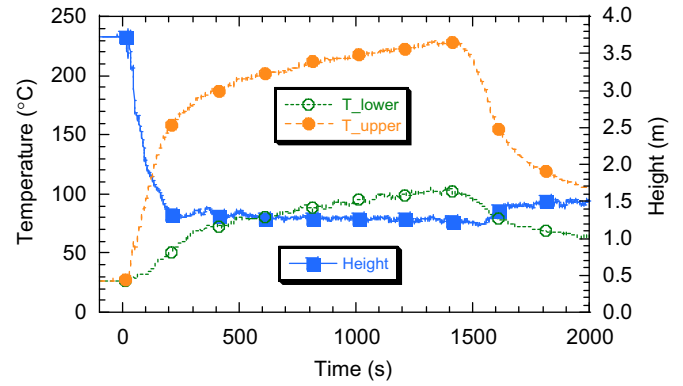


Fig. 5. The average temperature of the upper and lower layers and the layer height as a function of time on Tree 7.

above the floor) were used to estimate the uncertainty due to the influence of radiative exchange on the bare bead TC measurements. The aspirated measurement results showed that the temperature differences between the bare bead and the aspirated thermocouples varied during the test. The measured temperature differences were negligible in the hot smoky upper layer, but in the relatively cool lower layer, the differences increased during the test as the layer became hotter, with the aspirated TC measurements about 20 °C less than the bare bead results when the layer temperature was about 120 °C. When the fuel flow was shut and the fire size diminished, the difference between the aspirated and bare bead TC results decreased by about $\frac{1}{3}$ as compared to when the fire was burning. This was attributed to decreased radiative heat transfer to the bare bead TC from the fire, which was located about 2½ m from the edge of the fuel pan. Heat transfer to the bare bead TCs was complex and depended on the view factor of radiative emission from the fire, the walls, and the hot upper layer, in addition to transient convective heat transfer. Because the contribution of the lower gas layer enthalpy increase to the overall energy balance was relatively small, no attempt was made to correct the bare bead TC results for radiative exchange. Instead, radiative exchange was treated as part of measurement uncertainty. A conservative estimate of the lower layer temperature measurement uncertainty was taken as 20%, which contributed to a combined expanded uncertainty value of 8% for \dot{Q}_g in Eq. (4). The peak value of \dot{Q}_g was about 350 ± 30 kW. After 250 s, \dot{Q}_g was nearly zero, as heating of the compartment gases reached a quasi-steady value. The value of \dot{Q}_g relative to the other heat distribution terms is discussed further below.

4.2. Heat loss through the doorway

Fig. 6 shows the measured velocity profile along the centerline of the doorway as a function of time during the experiment. The bidirectional probes measured the flow in either direction. Positive and negative values signify flow into and out of the compartment, respectively. The lowest two probes recorded velocities into the compartment equal

to approximately 1.5 m/s during the fire. The probe located at the center fluctuated slightly above zero. The uppermost probes measured velocities equal to nearly -1 m/s (with a value less than zero indicating that flow was out of the compartment). The temperature and velocity measurements acquired at the doorway were used to compute the total heat loss through the doorway (\dot{Q}_d):

$$\dot{Q}_d \cong \sum_i \rho_i v_i A_i C_p \Delta T_i, \quad (5)$$

where A_i , ρ_i , v_i are the representative area, density, and velocity in the i th section of the doorway, C_p is the temperature dependent gas heat capacity (taken to be that of air), and ΔT_i is the increase in temperature from ambient. The value of ρ_i was computed from the doorway temperature measurements and application of the ideal gas law. The energy transport through the doorway was computed for each section of the doorway using local velocity and temperature measurements, and the summation over the entire opening was computed. Radiative loss through the doorway was assumed to be very small in this study for a fire that was far from the doorway in a very large enclosure.

The velocity measurements exhibited rather strong fluctuations at some locations. The data were time-averaged over a 30 s interval before determination of \dot{Q}_d . Since the emphasis of this study was during the steady burning period, the duration of the averaging was considered appropriate. Heat loss from the compartment was due to flow out of the room at locations above the neutral plane of the doorway. Below the neutral plane, relatively cool air flowed into the compartment, lowering the compartment enthalpy (with the magnitude of this correction about 1% as compared to the enthalpy flow out of the compartment). The neutral plane in the doorway varied as a function of time during the experiment, but was between 100 cm and 140 cm above the floor during the steady burning period as seen in Fig. 6. The probes at the 100 cm height that were off the centerline (on the north and south sides of the doorway opening) indicate flow out of

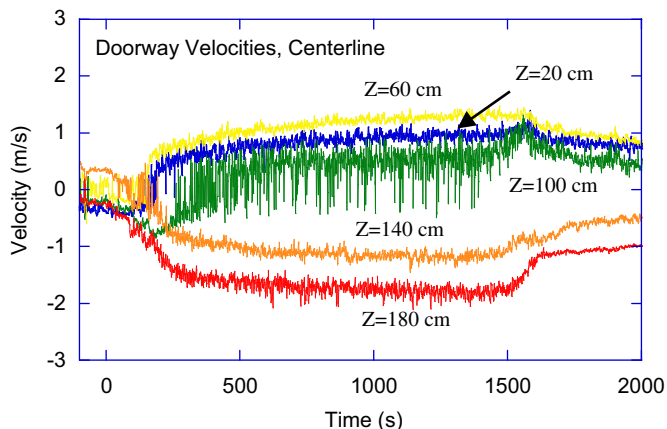


Fig. 6. Doorway velocities on the centerline at various heights (Z) above the floor.

the compartment, compared to a flow in as measured by the center probe at the 100 cm height. This suggests that the doorway flow had a “U” shape, consistent with other compartment doorway measurements [10].

The peak value of \dot{Q}_d was about 300 ± 20 kW, occurring just before the fuel was stopped at 1500 s. The value of \dot{Q}_d relative to the measured calorimetric heat release rate (\dot{Q}_f) is presented in Fig. 7. The figure also compares the results for both \dot{Q}_d and \dot{Q}_f in replicate experiments. While the calorimetric heat release rate was fairly steady after 500 s, the value of \dot{Q}_d continued to slowly increase from 500 to 1400 s, until its value enlarged by almost 35%. The combined expanded uncertainty in the enthalpy flow measurement was estimated as 13%, which was dominated by measurement variance and sensitivity to flow angle.

4.3. Heat loss to compartment surfaces

Fig. 8 shows the net heat loss rate as a function of time to each compartment surface. The sum of the loss to all of the walls is also shown. The pairs of symmetric walls (north/south; east/west) experienced nearly identical losses as would be expected. The largest losses were to the ceiling and the floor. Interestingly, the loss to the ceiling was not significantly different than that to the floor. As the upper layer heated, the temperature difference with the plume decreased and re-radiation from the ceiling was larger, so the net flux decreased. The flux to the floor increased during the fire, probably because the whole upper layer grew hotter, causing more radiative heating to the relatively cool floor. The value of \dot{Q}_w relative to the other heat distribution terms is discussed further below. Fig. 7 shows replicate experiments for \dot{Q}_f and \dot{Q}_d that indicate that the results were very repeatable.

4.4. Heat release rate

The calorimetric heat release rate measurement, \dot{Q}_f , as a function of time is shown in Fig. 9, as well as Fig. 7. Its value increased over the first 400–500 s of the experiment, and then became relatively steady. This was attributed to

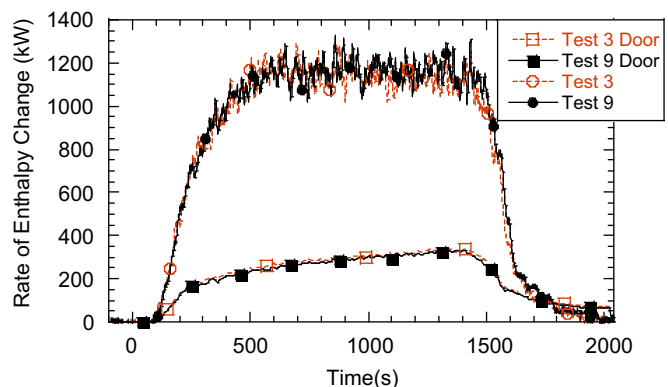


Fig. 7. The measured calorimetric heat release rate (\dot{Q}_f) and the enthalpy flow through the doorway (\dot{Q}_d) in repeat experiments.

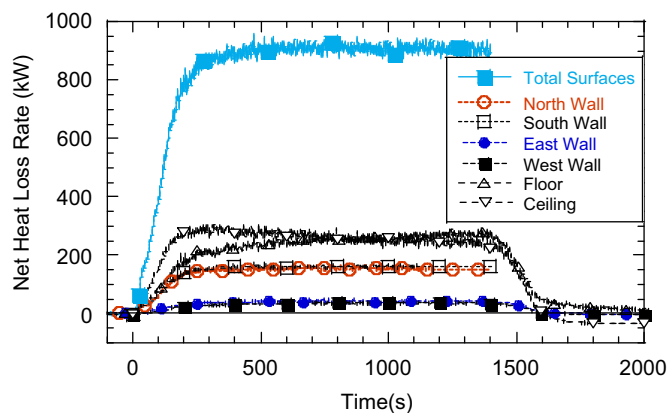


Fig. 8. Net heat loss rate to individual surfaces and their sum (\dot{Q}_d) as a function of time.

filling of the large volume of the test compartment with hot gases. The value of \dot{Q}_f decreased after approximately 1400s, when the fuel flow was ramped down. The maximum steady value of \dot{Q}_f determined by calorimetry was measured as $1140 \text{ kW} \pm 15\%$.

5. Conclusions

Fig. 9 considers the energy balance in the compartment as a function of time as represented by the energy loss to compartment surfaces (\dot{Q}_w), through the doorway (\dot{Q}_d), heating the gas phase (\dot{Q}_g), and the sum of these three terms. For comparison, the calorimetric heat release rate (\dot{Q}_f) is also shown. The sum of the heat loss terms during the steady burning period (from about 400s to about 1400s) slowly increased. The sum of the heat losses should be equal to the calorimetric heat release rate (see Eq. (1)). For early times ($t < 300$ s), the calorimetric results lagged the sum of the heat losses as the hot upper layer grew and obtained a quasi-steady temperature. The time lag was due to the measurement configuration in which the hot gases first filled the compartment and only then began to spill into the exhaust hood, where the heat release rate was measured. The uncertainty in the sum of the heat losses was estimated as 12%, whereas the uncertainty in the calorimetry was 15%. The agreement between the two curves was within the overlapping uncertainty limits. The mean value during the steady burning period of the sum of the heat losses was calculated as 1210 kW, which is within experimental uncertainty of the time-averaged value of the calorimetric measurement (1140 kW) during the steady burning period.

Integrating the area under the curves in Fig. 8 over the entire experiment showed that the total calorimetric heat release ($\int \dot{Q}_f dt$) was within 15% of the integrated value of the curves representing the sum of the distributed energy (i.e., $\int (\dot{Q}_g + \dot{Q}_w + \dot{Q}_d) dt$), which had a value equal to approximately 1.6 GJ. Nearly 74% of the fire energy went to heat compartment surfaces ($\int \dot{Q}_w dt$), 22% escaped

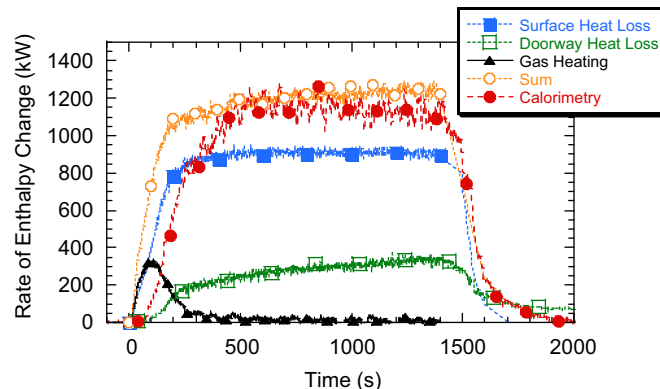


Fig. 9. The rate of heat loss to surfaces (\dot{Q}_w), through the doorway (\dot{Q}_d), accumulated by heating the gas (\dot{Q}_g), and their sum as a function of time. For comparison, the calorimetric heat release rate measurement (\dot{Q}_f) is also shown.

through the doorway ($\int \dot{Q}_d dt$), and 4% went to heat the compartment gases ($\int \dot{Q}_g dt$).

As previously noted [1], surface heat losses must be considered, if fire models are to accurately predict upper layer temperatures. The configuration, thermophysical properties, and conditions that characterize wall heat transfer should be considered when designing compartment fire experiments and applying fire models to the design of fire protection systems. Consideration of measurement uncertainty enables a confirmation of the conservation of energy, which provides a check on the quality of the individual measurements and lends confidence in the use of the data for model validation.

Acknowledgments

This work was co-sponsored by the US Nuclear Regulatory Commission and NIST. The authors are indebted to Lauren DeLauter, Edward Hnetovsky, Jack Lee, Jay McElroy, Roy McLane, and Mike Selepak for excellent technical assistance, and to Drs. Rodney Bryant, Kevin McGrattan, Tom Ohlemiller, and Jiann Yang for helpful discussions.

References

- [1] Walton WD, Thomas PH. Estimating temperatures in compartment fires. In: DiNenno PJ, et al., editors. SFPE Handbook of Fire Protection Engineering. 3rd Ed. Quincy, MA: National Fire Protection Association; 2002 (Section 3, Chapter 6).
- [2] Hamins A, Maranghides A, Yang J, Donnelly M, Mulholland G, Ohlemiller T, et al. Report of Test on Experiments for the International Fire Model Benchmarking and Validation Exercise #3." National Institute of Standards and Technology Special Publication 1013-1, Gaithersburg, MD; 2005. 157 pp.
- [3] Najafi B, Salley MH, Joglar F, Dreisbach J, Hill K, Peacock R, et al. Verification and validation of selected fire models for nuclear power plant applications. Rockville, MD: US Nuclear Regulatory Commission, Office of Regulatory Research (RES); Report No. NUREG-1824, Vol. 1–7, May 2007.
- [4] Salley MH, Joglar F, Dreisbach J, Hill K, Kasawara R, Najafi B, et al. Verification and validation—how to determine the accuracy of

- fire models. Fire Protection Engineering, The Society of Fire Protection Engineers, Spring 2007.
- [5] Hamins A, Maranghides M, Mulholland G. The global combustion behavior of 1 MW to 3 MW hydrocarbon spray fires burning in an open environment. National Institute of Standards and Technology Report NISTIR 7013; 2003. 13 pp.
- [6] Pitts WM, Braun E, Peacock RD, Mitler HE, Johnsson EL, Reneke PA, et al. Temperature uncertainties for bare-bead and aspirated thermocouple measurements in fire environments. National Institute of Standards and Technology (NIST) Report NISTIR 6242; 1998. 16 pp.
- [7] He Y, Fernando A, Luo M. Determination of interface height from measured parameter profile in enclosure fire experiment. Fire Safety J 1998;31:19–38.
- [8] McGrattan K (Ed.). Fire dynamics simulator (version 4) technical reference guide. National Institute of Standards and Technology Special Publication 1018; 2004. 110 pp.
- [9] McCaffrey BJ, Heskestad G. A robust bidirectional low-velocity probe for flame and fire application. Combust Flame 1976;26:125–7.
- [10] Bryant RA. A new approach to ventilation measurements in enclosure fires. In: Proceedings of the 11th international conference on fire science and engineering, London, England, September 2007, pp. 453–463.
- [11] Bryant R, Ohlemiller T, Johnsson E, Hamins A, Grove B, Guthrie WF, et al. The NIST 3 megawatt quantitative heat release rate facility. National Institute of Standards and Technology Special Publication 1007; 2003. 82 pp.